BNL-224788-2023-TECH

EIC-ADD-TN-067

MBTRACK2: A LONGITUDINAL RF BEAM LOADING TRACKING CODE

X. Gu

August 2023

Electron-Ion Collider

Brookhaven National Laboratory

U.S. Department of Energy

USDOE Office of Science (SC), Nuclear Physics (NP) (SC-26)

DISCLAIMER

MBTRACK2: A LONGITUDINAL RF BEAM LOADING TRACKING CODE

Xiaofeng Gu*
Collider Accelerator Department
Brookhaven National Lab
UPTON, NY 11973
xgu@bnl.gov

A. Gamelin
Synchrotron SOLEIL
Gif-sur-Yvette, France

August 21, 2023

ABSTRACT

In this paper, we present the introduction of Mbtrack2, a longitudinal RF tracking code, and provide a validation of its capabilities. We compare and verify the beam size and energy spread obtained from Mbtrack2 tracking with the theoretical results. Additionally, we present the results of the beam dynamics, considering the longitudinal beam loading effect. This includes the characterization of the energy spread, bunch length, and centroid offset as a function of the bunch number in the train. Furthermore, we discuss other features of Mbtrack2 code, such as robinson instability and beam equilibrium profile ect.

***K*eywords**

RF dynamics, beam loading, mbtrack2, RF instability

1 Introduction

In this paper, we introduce a Python code called Mbtrack2 [1], which has been validated with theory, although some instability features of the code have been benchmarked [2]. The code, developed at SOLEIL, is a

*xgu@bnl.gov,

coherent object-oriented framework written in Python for analyzing collective effects or beam-induced loading effects in an electron storage ring. The tracking model of Mbtrack2 is based on mbtrack, a C multi-bunch tracking code initially developed at SOLEIL. Mbtrack2 consists of different modules that allow for easy script writing for single bunch or multi-bunch tracking in a transparent manner.

In addition to beam-loading calculations, the Mbtrack2 code also includes methods to evaluate beam instability. For single bunch instability [3], it can calculate Micro Wave Instability, Transverse Mode-coupling Instability, and Headtail Instability. For multi-bunch instability, it includes the Resistive Wall Induced Coupled-bunch Instability and Robinson Instability modules. The general calculations related to instability included in Mbtrack2 are listed below.

* Compute the microbunching instability (MBI) threshold for a bunched beam considering the steady-state parallel plate model [4][5].
* Compute the longitudinal and transverse coupled bunch instability thresholds driven by higher-order modes (HOMs) [6][7].
* Compute the threshold current of the transverse coupled-bunch instability induced by resistive wall impedance [8].
* Compute the rise time of fast beam ion instability [9][10][11].
* Compute Robinson Instability [12].

The paper is organized as follows. The first section of this paper cites the formulas for beam length and energy spread in a storage ring. The subsequent section presents the beam-induced voltage in a storage ring. In the last section, we calculate and compare the results of bunch length, energy spread, and beam-induced voltage obtained from the Mbtrack2 code with the theoretical results from the previous sections.

2 Some Formulas in A Strorage Ring

2.1 Bunch length and Energy Spread in A Strorage Ring

In the paper, the 5 GeV ESR lattice (version 5.3, Bmad format) is used for all studies. The lattice parameters are listed in Table 1. The energy loss per turn U_0 in the table is given by

$$U_0 = \frac{C_\gamma E_0^2 I_2}{2\pi} \tag{1}$$

while $C_\gamma \approx 8.846 \times 10^{-5} m/GeV^3$.

The natural energy spread σ_δ and bunch length σ_z are given by:

$$\begin{aligned} \sigma_\delta^2 &= Cq\gamma^2 \frac{I_3}{J_z I_2} \\ \sigma_z &= \frac{\alpha_p c}{\omega_s}\sigma_\delta \\ \omega_s &= \sqrt{\frac{-eV_c h\eta_p \cos\phi_s}{2\pi\beta^2 E_0}} \end{aligned} \tag{2}$$

while $C_q = 3.832 \times 10^{-13} m$ and ω_s is the sychrotron tune of the storage ring with cos conversion. According to Eq. 2, one can observe that the nature of the energy spread is determined by the lattice itself, while the bunch length is determinded by both the RF parameters and the lattice parameters. Later, the simulated beam length using mbtrack2 with various configurations will be compared with the aforementioned analytical bunch length formula.

Table 1: The parameters of 5 GeV ESR lattice calcualted from Bmad.

Parameters	value	unit	comments
E_0	5	GeV	Energy
L	3833.930	m	length
I_0	2.5	A	Average beam current
M	580		number of bunches
Q_x	40.120006		Tune
$Chrom_x$	1.195723		dQ/(dE/E)
J_x	1.004150		Damping Partition
ϵ_x	2.54404×10^{-8}	m rad	Emittance
α_x	9.55030×10^{-5}		Damping per turn
τ_x	1.33908×10^{-1}	Sec	Damping Time
Q_y	37.100001		Tune
$Chrom_y$	0.804365		dQ/(dE/E)
J_y	0.999908		Damping Partition
ϵ_y	2.89894×10^{-14}	m rad	Emittance
α_y	9.50996×10^{-5}		Damping per turn
τ_y	1.34476×10^{-1}	Sec	Damping Time
Q_z	6.25245E-02		Tune
σ_δ	5.18657E-04		equilibrium energy spread
U_0	9.51083E+05	eV/turn	Energy Loss
J_z	1.99503E+00		Damping Partition
α_z	1.89744E-04		Damping per turn
τ_z	6.73993E-02	second	Damping time
α_p	1.33646E-03		Momentum Compaction
η_p	1.33645E-03		Slip factor
γ_t	2.73540E+01		Gamma at transition
$I0$	1.15168E+05		synchrotron integral
$I1$	5.12889E+00		synchrotron integral
$I2$	1.08084E-01		synchrotron integral
$I3$	1.56153E-03		synchrotron integral

2.2 Beam-Induced Voltage in A Storage Ring

In this section, we will cite some basic and useful formulas regarding the beam loading effect, primarily adapted from the reference [12]. These formulas will be utilized in the mbtrack2 code. It is important to note that these formulas employ sine conversion, while a reference [13] employs cosine conversion for verification.

Table 2: Some RF parameters and Their Description

Parameter symbol	Description
V_c	Voltage across the RF cavity gap
V_b	beam-induced voltage at resonance
I_g	generator current (transformed to the gap)
I_b	rf component of the beam current, image beam current at f_c. $I_b = 2I_0$ for shot bunches.
I_0	generator current needed to produce V_c when the cavity is at resonance without beam current
R_s	shunt resistance of the whole accelerating system (cavity, transmitter and beam load)
f_g	RF generator frequency
f_c	cavity resonant frequency
f_0	revolution frequency of the synchroniezed beam particles
ω_g	RF generator angular frequency
ω_c	cavity resonant anglular frequency
ω_0	angular revolution frequency of the synchroniezed beam particles
θ_s	stable phase angle for very short bunches measured from zero crossing of rf wave
ψ	phase between total current or cavity current and cavity voltage V_c, the detuning angle.
h	the rf harmonic number
N_b	the equal bunches number in the ring seperated equally by h_b
β	cavity coupling coefficient

2.2.1 Transient Beam Loading in RF frame for Equally Spaced Bunches

In this section, we derive the induced-voltage buildup from the transient state. Let the bunch spacing be denoted as ΔT_b in time. The filling time or cavity time constant is represented as T_f, and the e-folding voltage decay decrement between two successive bunch passages is denoted as τ. They can be expressed as follows:

$$T_f = \frac{2Q_L}{\omega_c} \tag{3}$$

$$\tau = \frac{\Delta T_b}{T_f} \tag{4}$$

where ω_c is the frequency of RF cavity. For the calculation of beam-induced voltage in the RF generator frame, the reference is chosen such that the voltage V_{b0} induced by each of the bunches lies along the negative real axis. During this time period, the phase of the RF cavity fields changes by $\omega_c \Delta T_b$, while the phase of the RF generator changes by $\omega_{rf} \Delta T_b$. Here, ω_{rf} represents the frequency of the RF generator.

Consequently, between successive bunches, the induced cavity voltage experiences a phase slip (relative to an RF generator frame that rotates as $e^{j\omega t}$), or its phasors rotate by an angle of $\delta \Delta T_b$. The slippage factor δ and this angle can also be expressed in terms of the detuning angle ψ.

$$\delta = (\omega_c - \omega_g) \tag{5}$$

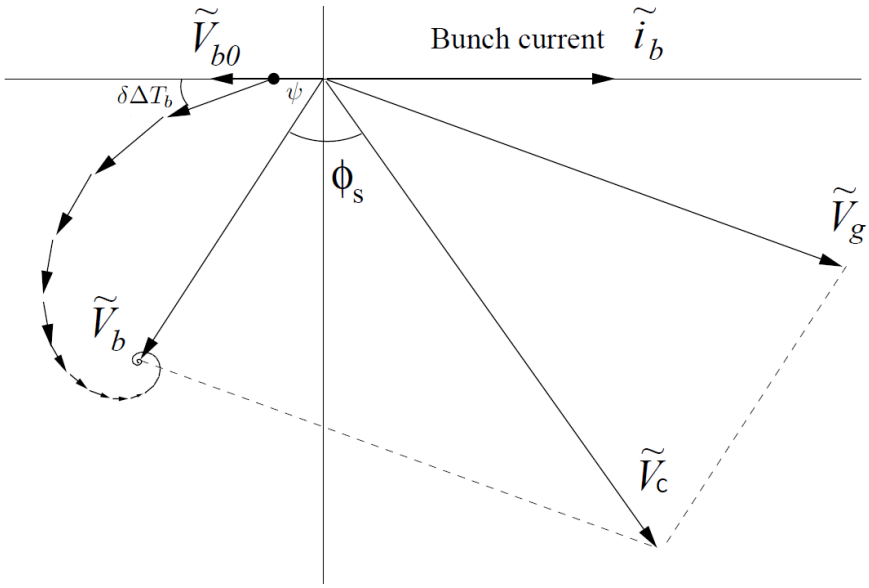

Fig. 1: Diagram illustrating the accumulation of transient beam-induced voltages in a cavity due to a sequence of evenly spaced bunches. Each preceding voltage phasor exhibits a phase advance or phase slip $\delta\Delta T_b$ or $e^{j\delta\Delta T_b}$ caused by detuning, as well as an amplitude decay of $e^{-\tau}$. It is important to note that the bunch currently passing by experiences only half of its induced voltage, $\frac{V_{b0}}{2}$. These voltage phasors combine to form the overall beam loading voltage phasor $\hat{V_b}$.

$$tan(\psi) = \frac{\delta\Delta T_b}{\tau} = 2Q_L\frac{\omega_c - \omega_g}{\omega_c} \tag{6}$$

Fig. 1 illustrates the buildup of beam-induced voltage in a cavity caused by a series of equidistant bunches. It can be observed from Fig. 1 that $\delta\Delta T_b$ represents the relative angle between successive bunches, rather than an absolute angle with respect to the original coordinate system. This coordinate system is referred to as the RF frame in the mbtrack2 code.

In addition to the phase shift, the induced voltage amplitude also decays in length by a factor of $e^{-\tau}$. When a short bunch carrying a charge q passes through, it generates a transient beam loading voltage denoted as V_{b0}, which can be mathematically expressed as:

$$V_{b0} = \frac{q}{C} = q\omega_c\frac{R_L}{Q_L} = 2k_l q = I_0\Delta T_b\omega_c\frac{R_L}{Q_L} = 2I_0R_L\tau \tag{7}$$

Where k_l is the cavity loss factor and can be written as:

$$k_l = \frac{\omega_c R_L}{2Q_L} \tag{8}$$

As subsequent short bunches pass through the same region, they also contribute to the beam loading voltage. The total beam loading voltage, denoted as V_b, is obtained by vectorially adding up the beam loading voltage

phasors for all previous bunch passages. They can be expressed as:

$$\hat{V_b} = \frac{1}{2}V_{b0} + V_{b0}\left(e^{-\tau}e^{j\delta\Delta T_b} + e^{-2\tau}e^{2j\delta\Delta T_b} + e^{-3\tau}e^{3j\delta\Delta T_b} + ...\right) \tag{9}$$

Finally, we can obtain the beam-induced voltage for an equally spaced full ring using Equation 9.

$$\hat{V_b} = V_{b0}\left(\frac{1}{1 - e^{-\tau}e^{j\delta\Delta T_b}} - \frac{1}{2}\right) \tag{10}$$

Wilson's fundamental theorem of beam loading states that a particle in a cavity experiences only half of its own induced voltage, which is represented as the $\frac{1}{2}$ term in the equation above. This induced voltage arises from the excitation of the cavity and oscillates at the resonant frequency of the cavity. It is worth noting that higher-order modes of the cavity are not considered in this analysis.

2.2.2 Steady-State Beam Loading in Beam frame

In the previous sections, the derivation of the beam-induced voltage buildup in a resonant cavity was presented based on first principles, eliminating the requirement for an external RF generator. In this scenario, it is appropriate to select a reference phase that aligns the beam-induced voltage at resonance with the negative real axis.

However, when a voltage component from an RF generator is present in phasor diagrams and the beam-induced voltage has been accumulated, it is customary to position the net cavity voltage along the positive real axis, as depicted in Figure 2. This alignment coincides with the placement of the beam current phasor and is referred to as the beam frame within the mbtrack2 code.

In this paper, the beam frame is utilized for simulating beam-induced voltage and beam-loading effects. On the other hand, the RF frame is exclusively employed for calculating the initial beam-induced voltage. In

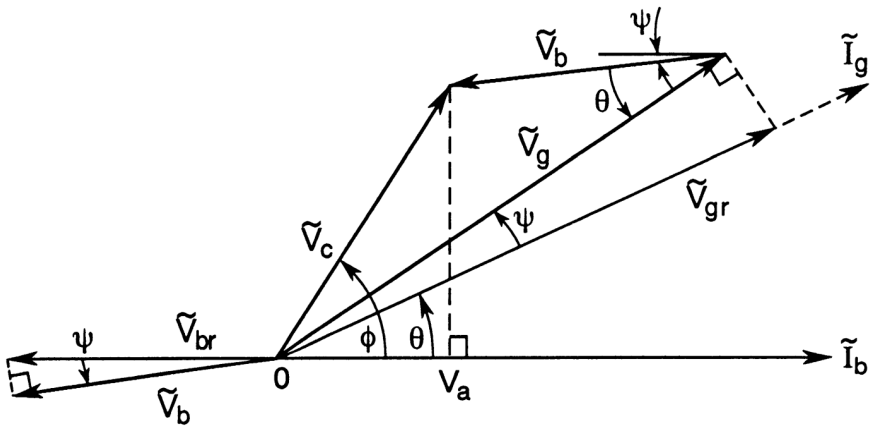

Fig. 2: Diagram depicting the vector addition of the generator and beam loading voltage in an RF cavity.

this frame, the projection on the positive axis of the cavity voltage, located at the synchronous phase angle ϕ,

represents the accelerating component of the cavity. The generator current I_g, whose phase aligns with the generator-induced voltage at resonance $\hat{V}_{gr}$, is inclined at an angle θ with respect to the real axis (and with respect to the beam current, I_b).

In the beam frame, the induced voltage amplitude decays in length by a factor of $e^{-\tau}$, similar to the RF frame. However, in this case, the phase slippage factor is denoted as δ, which currently is given by:

$$\delta = \omega_c \tag{11}$$

In the limit of small τ and small δ, Eq. 10 can be rewritten with the assistance of Eq. 6 and Eq. 7 as follows:

$$\begin{aligned} \hat{V}_b &= 2I_0 R_L cos(\psi) e^{j\psi} \\ V_{br} &= 2I_0 R_L = \frac{2I_0 R_s}{1+\beta} = I_b R_L = \frac{V_{b0}}{\tau} \\ \hat{V}_b &= V_{br} cos(\psi) e^{j\psi} \end{aligned} \tag{12}$$

Meanwhile, the generator voltage can be expressed as:

$$\begin{aligned} V_{gr} &= I_g R_L = \frac{2\beta^{1/2}}{1+\beta} \times (2RP_g)^{1/2} \\ \hat{V}_g &= V_{gr} cos(\psi) e^{j\psi} \end{aligned} \tag{13}$$

While the cavity voltage can be expressed as:

$$\hat{V}_c = \hat{V}_b + \hat{V}_g \tag{14}$$

The real (accelerating) and imaginary components of the net cavity voltage are as follows:

$$\begin{aligned} V_R &= V_c cos\phi = V_{gr} cos\psi cos(\theta+\psi) - V_{br} cos\psi^2 \\ V_I &= V_c sin\phi = V_{gr} cos\psi sin(\theta+\psi) - V_{br} cos\psi sin\psi \end{aligned} \tag{15}$$

Using Eq. 12, Eq. 13 and Eq. 15, The required generator power, expressed in terms of V_c and ϕ, for a given cavity detuning angle ψ and coupling β, can be written as follows:

$$\begin{aligned} P_g &= \frac{(1+\beta)^2}{8\beta R_s} V_{gr}^2 \\ &= \frac{(1+\beta)^2}{8\beta R_s} V_c^2 \left[\left(\frac{cos\phi_s}{cos\psi} + \frac{V_{br}}{V_c} cos\psi \right)^2 + \left(\frac{sin\phi_s}{cos\psi} + \frac{V_{br}}{V_c} sin\psi \right)^2 \right] \end{aligned} \tag{16}$$

Another similar method for obtaining the power consumption of the RF generator mentioned above has been described in [13]. The detailed procedure is provided in Appendices A and B, using different notation.

2.2.3 Steady-State Beam Loading Optimization

The adjustment of the RF system must be performed in such a way as to provide the desired energy gain for synchrotron energy loss U_0.

Meanwhile, in order to increase the efficiency of a generator, it is advantageous for the phasors of the generator current $\hat{I_g}$ (and therefore $\hat{V}_{gr}$) and the RF voltage $\hat{V_c}$ to be aligned in the same direction. This alignment ensures that the load appears as purely resistive to the generator, minimizing the amount of energy stored in the system. Thus, the energy flow from the generator to the cavity is maximized, and the reflected voltage from a beam-loaded cavity will appear real. From Figure 2, this implies that $\theta = \phi$, and it can be achieved by changing the detuning angle ψ.

By utilizing this condition and applying the law of sines to the phasor triangle, we can obtain the optimum operating parameters, which are listed below:

$$\beta_0 = 1 + \frac{2I_0R_s cos\phi}{V_c} = 1 + \frac{P_b}{P_c} \tag{17}$$

$$tan\psi_0 = -\frac{V_{br}}{V_c} sin\phi \tag{18}$$

$$\begin{aligned} V_{gr0} &= V_c + V_{br} cos\phi \\ P_{g0} &= \frac{(1+\beta)^2}{8\beta R_s} V_{gr0}^2 \end{aligned} \tag{19}$$

The compensation scheme involving detuning is more effective compared to the scheme without it. This is because a portion of the beam loading voltage is utilized for the RF cavity voltage, and the current generated by the generator is synchronized with the RF cavity voltage. Consequently, the power required by the generator is reduced compared to the case where detuning is not employed.

Taking the derivative of Eq. 16 with respect to the detuning angle demonstrates that the generator's power reaches its minimum value when the phasors of the generator's current and the RF voltage are in-phase. In situations where the beam intensity is extremely high, the voltage V_b for beam loading may significantly exceed the necessary gap voltage V_c.

To achieve optimal performance when using the mbtrack2 code for tracking, the following procedure must be followed:

* First, we should set the coupling β to optimal value via Eq. 17;.
* then set the detuning angle to optimal conditions via Eq. 18;
* finally, we set generator parameters P_g via Eq. 16 , V_{gr} via Eq. 13, θ_{gr} via Eq. 15, V_g via Eq. 12 and $\theta_g = \theta_g + \psi$ for a given current and other RF parameters.

2.3 Robinson Instability

In this section, we present the theory concerning the Robinson Instability, which encompasses two distinct types of stability limits [14]. The first criterion for Robinson stability is impedance limitation or phase oscillation stability, which indicates that the detune frequency should be increased or decreased in comparison with $h\omega_0$. The second criterion for Robinson stability is RF power limitation, aiming to reduce the RF power requirement.

2.3.1 Phase Instability and Impedance Limitation

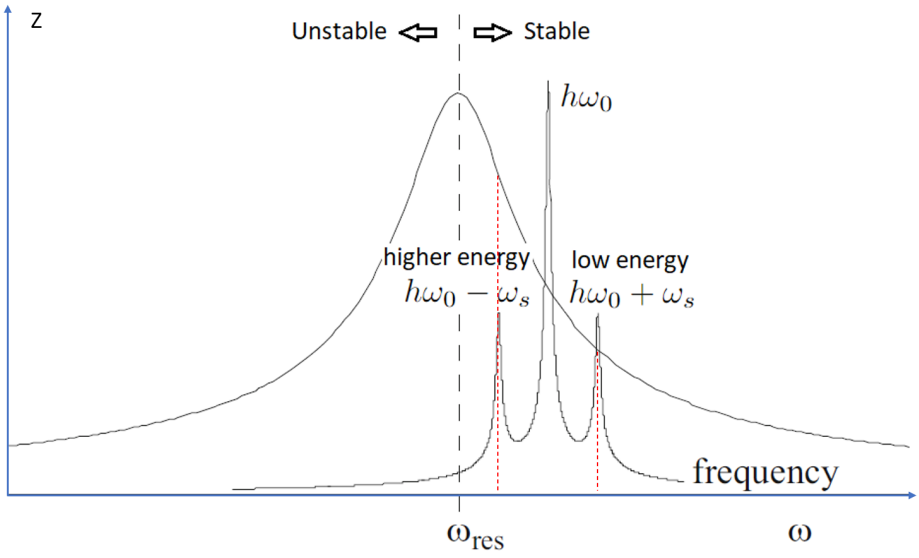

Fig. 3: Cavity tuning for positive Robinson damping above transition energy. The cavity frequency is moved to the left side of h harmonic order of revolution frequencey.

To achieve stable phase oscillations, it is necessary to set the correct synchronous phase, which depends on whether the particle energy is below or above the transition energy. Robinson found that phase stability for particles above the transition energy requires the RF voltage to decrease with increasing phase.

For energies above the transition energy, the revolution frequency is lower for higher bunch energies compared to the reference energy, and vice versa. To damp coherent phase oscillations, the cavity must be tuned such that the bunch loses more energy in the cavity at higher energies (lower frequency) during the course of coherent synchrotron oscillation, and loses less energy at lower energies (higher frequency).

Therefore, the first Robinson stability criterion is a tuning angle $\psi < 0$ for energies above the transition energy. The cavity resonace frequence is tuned to the left side of $h\omega_0$. Fig. 3 demonstrates that the impedance of the cavity should decrease with increasing frequency for damping to occur. And it can be demonstrated to be the reverse below the transition energy.

For a more detailed discussion on the qualitative and quantitative approaches to phase instability, refer to the following references: [14], [15], [16].

2.3.2 RF Power Or Voltage Limiation

The second stability limit arises due to the constraint imposed by the available RF power. Referring to Fig. 2, we observe that the phase of the generator voltage component relative to the beam is denoted as $\theta + \psi$. Consequently, the condition $dV_g/dt < 0$ yields $sin(\theta + \psi) > 0$. Alternatively, using Eq. 15, we can derive the following expression:

$$2V_c sin\phi + V_{br} sin2\psi > 0 \tag{20}$$

Furthermore, if the cavity tuning is adjusted to ensure the beam-loaded cavity voltage appears real, and if the cavity coupling is also optimized, then the second Robinson instability criterion can be expressed as follow:

$$V_c > V_{br} cos\phi \tag{21}$$

which the Robinson stability criterion conditioin is always satisfied in Mbtrack2 [12].

3 Mbtrack2 Validation

3.1 Beam Tracking in Mbtrack2

Mbtrack2 is a tool that handles RF cavities and longitudinal beam dynamics, considering the influence of the RF generator and beam loading effects. To accomplish this, it employs the cosine convention for RF voltage. The treatment of cavity physics in Mbtrack2 follows the phasor formalism established in reference [1]. For detailed insights into the implementation and benchmarking, please refer to references [17] and [18].

3.1.1 RFCavity Tracking Method

There are two main methods in the tool that handle this: RFCavity and CavityResonator. The RFCavity method is a simple one used for tracking, which models RF cavities using a perfect cosine wave. With this method, all macro-particles in a bunch can be tracked with a single mathematical operation.

The track algorithm of the RFCavity method can be called for both Bunch and Beam elements, and it simply applies:

$$\delta = \delta + \frac{V_c}{E_0} \cos(m\omega_g \tau + \theta) \tag{22}$$

Here δ denotes the energy spread.

The plot shows the bunch length (top), energy spread (bottom left), and longitudinal emittance (bottom right) as a function of tracking turns for three different initial beam sizes. The RFCavity method is used during the

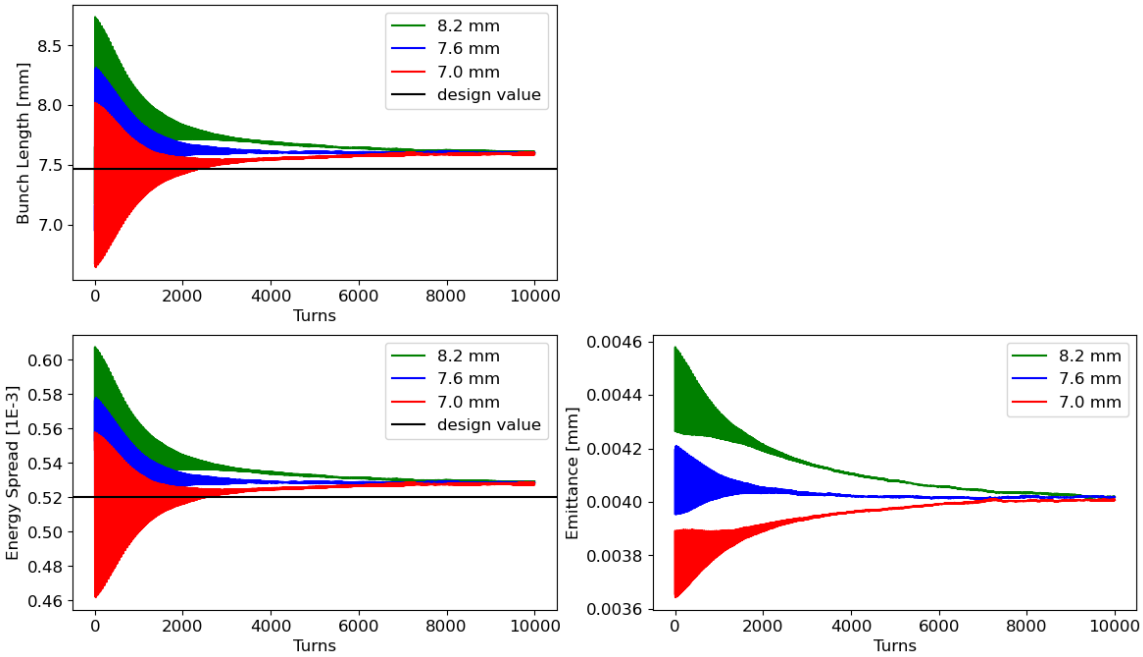

Fig. 4: The plot illustrates the bunch length (top), energy spread (bottom left), and longitudinal emittance (bottom right) as a function of tracking turns for three different initial beam sizes 7.0mm, 7.6mm and 8.2mm, while the energy spread is kept same.

tracking process. It can be observed that the three different initial beam sizes converge to a single value after 10k turns.

A similar benchmark was also carried out using SOLEIL II parameters. The energy spread, bunch length, and emittance tracking with the mbtrack2 code also agree very well with theory [19].

3.1.2 CavityResonator Tracking Method

On the other hand, the CavityResonator method is the primary approach utilized for self-consistently modeling RF cavities, taking into account beam loading. In this method, the bunch is divided into multiple bins, and the macro-particles within each bin are tracked simultaneously. Consequently, this method exhibits slower performance compared to the RFCavityh method. Nonetheless, the CavityResonator method proves useful for modeling active RF cavities, passive RF cavities, and HOM cavities in tracking.

The tracking process employing the CavityResonator method relies on the cavity phasor, which represents the phasor summation of the generator phasor and the beam phasor. The generator phasor is defined by the generator voltage V_g and phase θ_g:

$$\hat{V}_g = V_g e^{j(m\omega_g \tau + \theta_g)} \tag{23}$$

In the context of beam dynamics, the beam phasor undergoes dynamic evolution during each operation of the bins, which is dependent on the positions and charges of the macro-particles.

The beam phasor, denoted as $\hat{V}_b$, is constructed through the successive passages of various particles within the cavity. Longitudinally, each bunch is divided into bins, and as a bin of charged particles passes through the RF cavity, it induces a voltage.

$$\hat{V}_0 = -2k_l q_{mp} N_{mp} \tag{24}$$

Where k_l is the cavity loss factor, q_{mp} is the macroparticle charge, and N_{mp} is the number of macropartiles in the bin.

The total voltage induced by the particles crossing the cavity is the result of summing the present beam-induced voltage $\hat{V}_0$ with the previous voltage $\hat{V}_b(t)$ in the cavity at time t after Δt time of amplitude and rotation angle decay.

$$\hat{V}_b(t + \Delta t) = \hat{V}_b(t)e^{-\tau}e^{j\delta\Delta t} + \hat{V}_0 = \hat{V}_b(t)e^{-\tau}e^{j\delta\Delta t} - 2k_l q_M \tag{25}$$

Where τ is defined in Eq. 4 and δ is the phase slippage factor, as mentioned in previous sections. The simulated/tracked beam-induced voltage in the beam frame via Eq. 25 will be compared with the analytical formulas in Eq. 9 and Eq. 10.

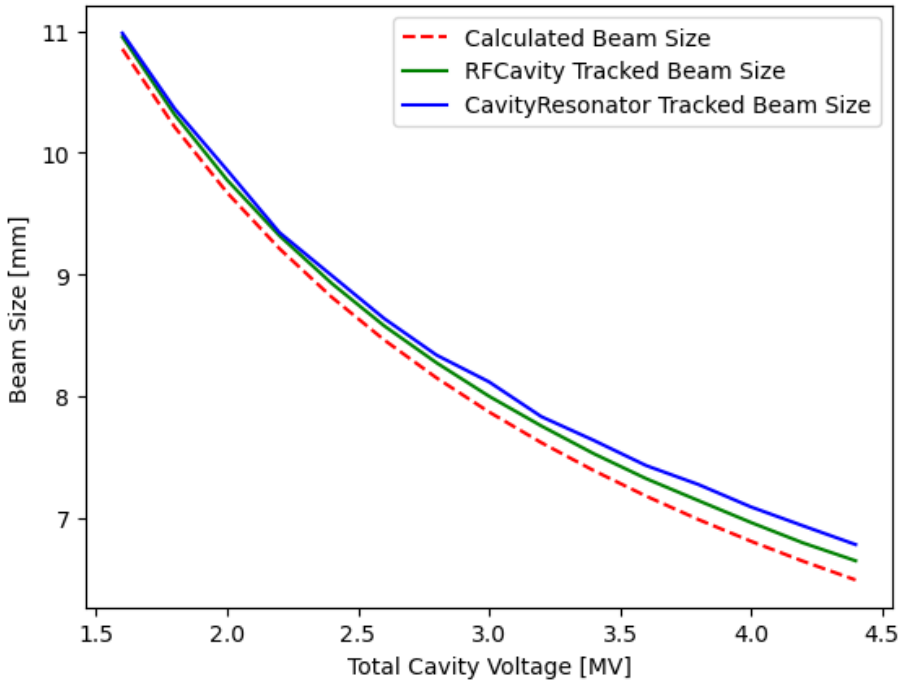

Fig. 5: The plot depicts the relationship between the bunch length and RF cavity voltage for two methods: the RFcavity method (represented by the green curve) and the CavityResonator method (represented by the blue curve). The corresponding theoretical results for each method are shown as dashed lines.

As a particle see only half of its wake, the energy change felt by the particles in the bin is:

$$\delta = \delta + \frac{q}{E_0}\left[Re[\hat{V}_g] + Re[\hat{V}_b] - q_M k_l\right] \tag{26}$$

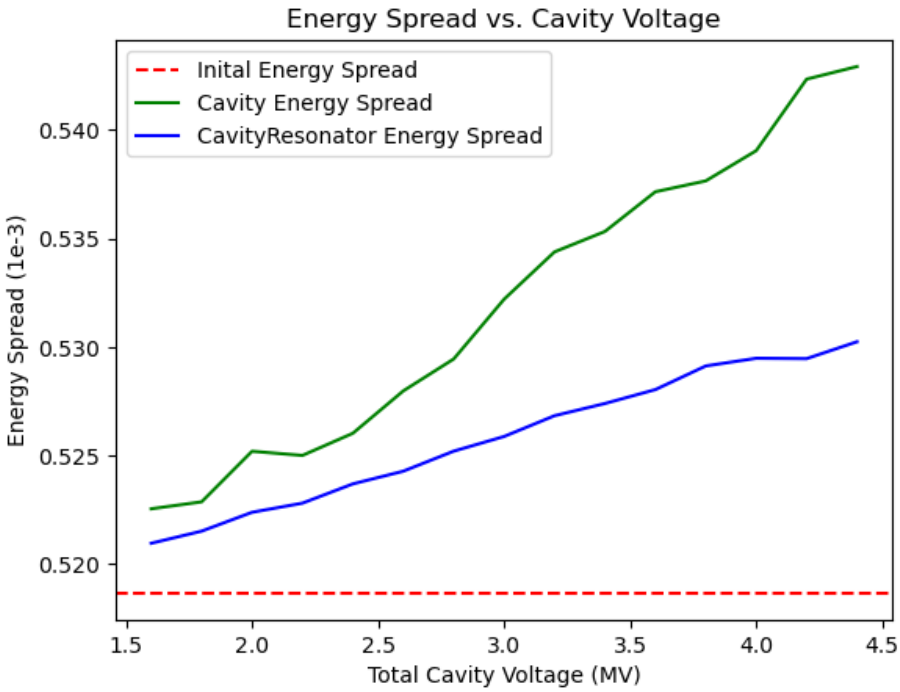

Fig. 6: The plot depicts the relationship between the energy spread and RF cavity voltage for two methods: the RF cavity method (represented by the green curve) and the Cavity Resonator method (represented by the blue curve). The corresponding theoretical results for each method are shown as dashed lines.

At the initialization of the CavityResonator, the beam phasor is set to zero.

3.1.3 One Turn Tracking Map

The one-turn tracking map in the mbtrack2 code includes a particle's longitudinal position and energy map. The phase space employed in the mbtrack2 code is represented by (τ, δ), which corresponds to the domain of time and energy spread. The variation in energy spread caused by synchrotron radiation is given by:

$$\delta = \delta - \frac{U_0}{E_0} \tag{27}$$

while the energy spread change becuase of radiation damping and quantum excitation can be expressed as:

$$\delta = (1 - \frac{2T_0}{\tau_z})\delta + 2\sigma_\delta(\frac{T_0}{\tau_z})^{0.5} \times rand \tag{28}$$

To save some compuation time with Mbtrack2, Eq. 26, Eq. 27 and Eq. 28 could be put together within one line and we can get the energy spread one turn map as:

$$\delta = (1 - \frac{2T_0}{\tau_z})(\delta - \frac{U_0}{E_0}) + 2\sigma_\delta(\frac{T_0}{\tau_z})^{0.5} \times rand + \frac{q}{E_0}\left[Re[\hat{V}_g] + Re[\hat{V}_b] - q_M k_l\right] \tag{29}$$

While one turn longitudinal map including the beam position is:

$$\sigma_z = \sigma_z + \eta_p T_0 \delta \tag{30}$$

here η_p is the frequency slip factor and T_0 is the revolution time.

3.2 Bunch Length and Energy Spread Validation with Mbtrack2 Tracking

First, we validate the beam length tracking in Mbtrack2 by comparing the results with the theoretical formula, Eq. 2. We track the beam lengths as a function of RF cavity voltage using both the RFcavity and CavityResonantor methods (both without beam loading effect).

Fig. 5 depicts the beam length as a function of RF cavity voltage for different tracking methods and their theoretical results. It can be observed that the tracking results agree very well with the theoretical results for moderate cavity voltages. However, for high cavity voltages, the tracking results begin to diverge (less than 5 percent) from the theoretical results, possibly due to over-focusing by the cavity. Therefore, we should avoid over-focusing of the RF cavity.

Fig. 6 depicts the beam energy as a function of RF cavity voltage for different tracking methods and their theoretical results. It can be observed that the beam energy spread increases with high cavity voltage, reaching approximately 4 percent and 2 percent for the RFCavity and CavityResonator methods, respectively. Nevertheless, the results still agree well with each other.

From the beam length and energy spread tracking, we can conclude that the Mbtrack2 code accurately handles the beam length and energy spread.

There is a deviation of several percent between the simulation and theory, which may arise from two reasons. The first reason is the possible initial beam mismatch with the RF bucket. As we know, for a fixed energy of the Hamiltonian, we can obtain the phase space shape of a particle, which consists of sets of ellipses.

$$\begin{aligned} \left(\frac{\delta}{\hat{\delta}}\right)^2 + \left(\frac{\varphi}{\hat{\phi}}\right)^2 &= 1 \\ \frac{\hat{\delta}}{\hat{\phi}} &= -\frac{Q_s}{h|\eta|} \end{aligned} \tag{31}$$

Where $\varphi = \phi - \phi_s$, $\hat{\delta}$ and $\hat{\phi}$ represent the maximum amplitudes of the phase-space ellipse. The phase area of the ellipse is given by $\pi\hat{\delta}\hat{\phi}$. Further details about Eq. 31 can be found in the reference [21].

By examining Eq. 31, we observe that the energy and longitudinal phase or position of particles reside on the ellipses in the phase space, following the rule described by Eq. 31. However, during the initial generation of macro-particles, these two dimensions are randomly and independently generated. As a result, a discrepancy

arises between them, which can be observed as a discrepancy between the Cavity method and the theoretical results.

Another factor that may contribute to this discrepancy is the binning of the bunch. In the simulation using CavityResonator, the bunch is divided into bins. The number of bins used for slicing the bunch has an impact on the simulated beam length and energy, which will be demonstrated later.

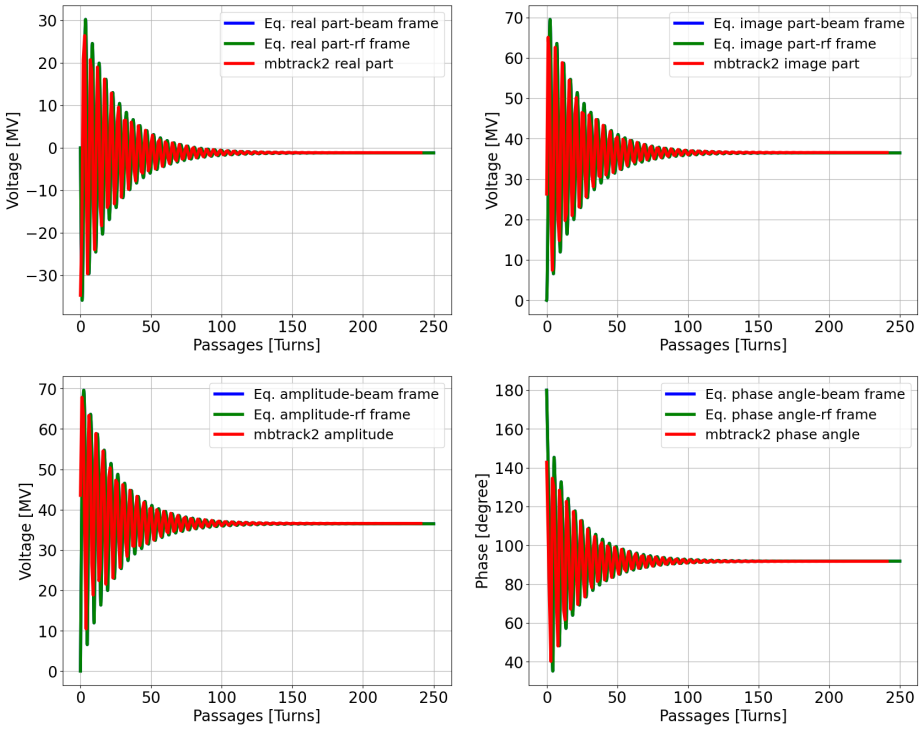

Fig. 7: The plot shows the beam-induced voltage calculated with formula in beam-frame and RF-frame, asn well as from the Mbtrack2 tracking.

Table 3: Induced voltages and phase angles

	Real [MV]	Imag [MV]	Phase Angle [degree]
formula	-1.1524	36.4904	91.8089
iteration	-1.1896	36.4894	91.8673
mbtrack2	-1.1384	36.5822	91.7824

3.3 Beam Loading Validation with Mbtrack2 Tracking

In this section, we first validate the beam-induced energy using the CavityResonator method by employing 1260 equally spaced bunches, with a total beam current of 2.5

A. Fig. 7 illustrates the beam-induced voltage as a function of tracking turns, calculated via the mbtrack2 initial phasor function, along with an iteration loop based on Eq. 9 within the RF frame and beam frame.

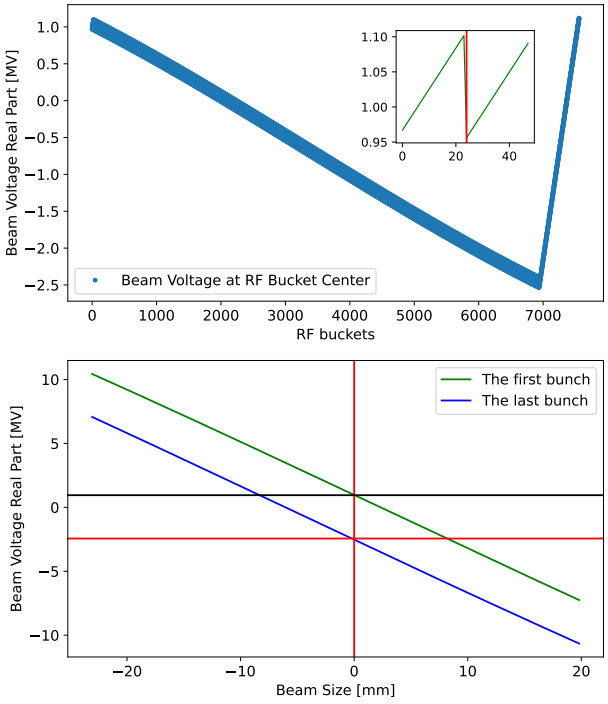

Fig. 8: The top plot shows the beam induced-voltage as function of the bunch train or RF buckets. The bottom plot shows the beam-induced voltage as function of longitudinal macropartile position in a bunch.

From the plot, we observe excellent agreement between the results obtained from mbtrack2 (red curve) and the others. The slight discrepancy at the beginning of tracking, where mbtrack2 differs from the others, arises due to the absence of beam-induced voltage data points at each bunch location in mbtrack2, while the other two methods incorporate this information. The parameters of the last data point for each method are listed in the table 3.

Based on the table 3 and the plot 7, it is evident that the calculated beam loading agrees very well with both theory and our self-developed iteration algorithm.

Next, we check the beam-induced energy using the CavityResonator method with 290 equally spaced bunches, where 24 empty buckets are present between each bunch. Additionally, there is an empty gap at the end of the bunch train which contains 100 empty RF buckets.

The top plot in Figure 8 depicts the beam-induced voltage as a function of RF buckets for the first turn of tracking. The beam-induced voltage corresponds to the voltage at the center of each RF bucket, with 24 empty buckets separating each bunch. The zoomed-in plot on the top right of the figure reveals that the initial beam-induced voltage is approximately 0.97 MV after the first bunch. Subsequently, the voltage decays with

time, encompassing both amplitude and angle. Due to the high Q-factor, the decay is predominantly governed by angle rotation rather than amplitude decay. Consequently, the voltage increases after passing through the 24 empty buckets. After passing the second bunch (the red vertical line), the beam-induced decrease again

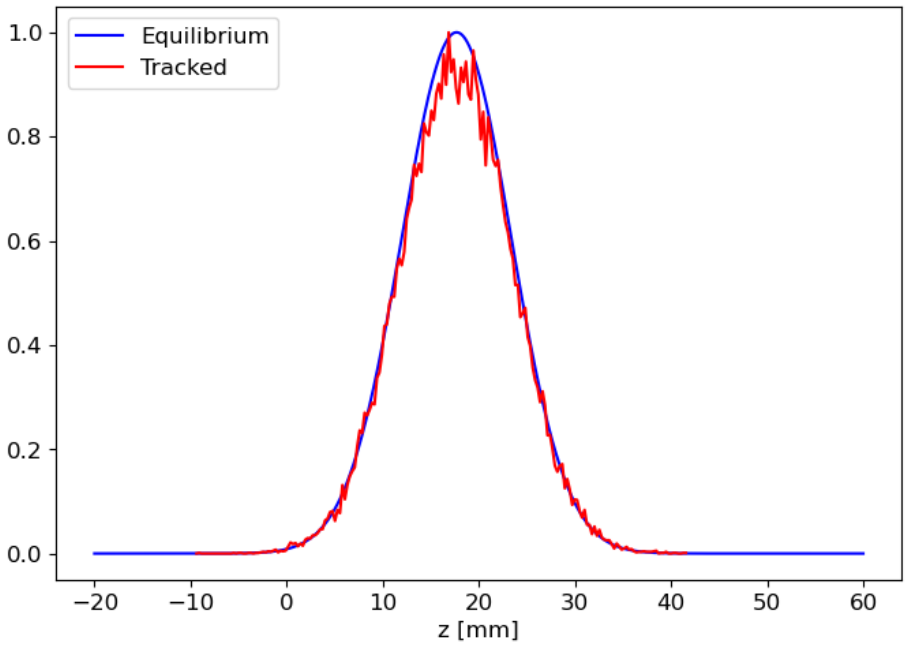

Fig. 9: The plot depicts the equilibrium profile calculated according to Ref. [20] and the tracked profile of the center bunch in the bunch train.

because of the induced voltage from this fresh bunch, and it increases again while going through the later empty RF buckets. This process is repeated 290 times, and the beam-induced voltage reaches about -2.44 MV. After that, it goes through another 100 empty bucket gap and starts another turn.

The bottom plot in Fig. 8 shows the beam-induced voltage inside (along) the first bunch (the green line) and the last bunch (the blue line). At the center (the vertical red line) of both bunches, their beam-induced voltages are 0.97 MV and -2.44 MV respectively (see also the top plot). The plot indicates that particles at different longitudinal beam locations will experience different beam-induced voltages.

If we extend the bunch length to cover the full length of the bucket, the bottom beam-induced voltage along the longitudinal position can be represented by a sine wave-like profile in the bottom plot of Fig. 8.

3.4 Equilibrium Profile and Position Validation

There is a method (formula) to obtain the equilibrium bunch density distribution [17] with an arbitrary number of active or passive RF cavities in a uniform filling pattern. The calculation method has been implemented in the Mbtrack2 code and compared with tracking [18].

The method covers the general case of an RF system with an arbitrary number of cavities, taking into account both beam loading and generator voltage. This approach can be applied to various scenarios, including the main RF cavity, passive and active harmonic cavities, with different phase, voltage, and harmonic settings.

To validate the final equilibrium profile and bunch position, a two RF cavity system with a reverse phase setting is used for the validation. The RF parameters for both cavities are listed in Table 4.

Fig. 9 illustrates the equilibrium profile and bunch position after 20k turns of tracking. The plot demonstrates that the Mbtrack2 tracking results exhibit good agreement with the theoretical calculations regarding the equilibrium profile and bunch longitudinal position (with an offset of approximately 17.5 mm).

Increasing the number of tracked macro-particles can further improve the deviation and reduce the noise in the curve around the tracked bunch center.

Table 4: RF parameters for mbtrack2 Simulation setup

Parameter	10 Focusing Cavity	5 Defocusing Cavity
m	1	1
N_{cav}	10	5
$R_{s\_per\_cavity}$ [Ω]	7.4e+11	7.4e+11
Q	2e+10	2e+10
Q_L	9.09944e+05	9.09944e+05
β	2.19784e+04	2.19784e+04
$detune$ [Hz]	-1.63399e+04	1.63404e+04
f_c [Hz]	5.91134e+08	5.91167e+08
ω_c [rad/s]	3.71421e+09	3.71441e+09
ψ [deg]	-88.86	88.86
V_c [V]	3.35e+07	1.675e+07
θ_s [deg]	88.86	-88.86
V_g [V]	1.33158e+06	6.65788e+05
θ_g rad	1.80814e-06	-1.80829e-06
V_{gr} [V]	6.6997e+07	3.34985e+07
θ_{gr} [deg]	88.86	-88.86
V_b [V]	3.35e+07	1.675e+07
V_{br} [V]	1.68552e+09	8.42759e+08
P_g [W]	1.66657e+06	8.33285e+05
P_c [W]	7.58277e+01	3.79139e+01
P_b [W]	1.66649e+06	8.33247e+05
P_r [W]	2.51703e-10	9.43601e-12
n_{bin}	200	200
R_s [Ω]	7.4e+12	3.7e+12
Filling time [s]	4.89980e-04	4.89953e-04
Loss factor [V/C]	6.87128e+11	3.43583e+11

4 Summary and Discussion

In this paper, we compared the bunch length, energy spread, and beam-induced voltage obtained from Mbtrack2 tracking with their theoretical values. We observed a high level of agreement between the two, indicating that the results from Mbtrack2 align well with the theoretical predictions. Additionally, the bunch equilibrium

profile and its longitudinal position, as obtained from Mbtrack2, also exhibit excellent agreement with the theoretical expectations. More Mbtrack2 benchmark can be found in the reference [2].

References

[1] https://gitlab.synchrotron-soleil.fr/PA/collective-effects/mbtrack2

[2] doi:10.18429/JACoW-IPAC2021-MOPAB070, IPAC2021, Campinas, SP, Brazi,

[3] doi:10.18429/JACoW-IPAC2021-MOPAB068, IPAC2021, Campinas, SP, Brazi,

[4] Y. Cai, "Theory of microwave instability and coherent synchrotron radiation in electron storage rings", SLAC-PUB-14561

[5] D. Zhou, "Coherent synchrotron radiation and microwave instability in electron storage rings", PhD thesis, p112

[6] Ruprecht, Martin, et al. "Calculation of Transverse Coupled Bunch Instabilities in Electron Storage Rings Driven By Quadrupole Higher Order Modes." 7th Int. Particle Accelerator Conf.(IPAC'16), Busan, Korea.

[7] Akai, Kazunori. "RF System for Electron Storage Rings." Physics And Engineering Of High Performance Electron Storage Rings And Application Of Superconducting Technology. 2002. 118-149. Eq. 51 p139

[8] R. Nagaoka and K. L. F. Bane, "Collective effects in a diffraction-limited storage ring", J. Synchrotron Rad. Vol 21, 2014. pp.937-960

[9] T. O. Raubenheimer and F. Zimmermann, "Fast beam-ion instability. I. linear theory and simulations", Physical Review E 52 (1995).

[10] G. V. Stupakov, T. O. Raubenheimer, and F. Zimmermann, "Fast beam-ion instability. II. effect of ion decoherence", Physical Review E 52 (1995).

[11] Chao, A. W., Mess, K. H. (Eds.). (2013). Handbook of accelerator physics and engineering. World scientific. 3rd Printing. p417.

[12] Wilson, P. B. (1994). Fundamental-mode rf design in e^+ e^- storage ring factories. In Frontiers of Particle Beams: Factories with e+ e-Rings (pp. 293-311). Springer, Berlin, Heidelberg.

[13] K.Y, Ng, https://lss.fnal.gov/archive/2002/fn/FN-0713.html

[14] R. Garoby, Beam Loading in RF Cavities.

[15] Helmut Wiedemann, Particle Accelerator Physics (Fourth Edition)

[16] Alexander Wu Chao, Physics of Collective Beam Instabilities in High Energy Accelerators

[17] Yamamoto, Naoto, Alexis Gamelin, and Ryutaro Nagaoka. "Investigation of Longitudinal Beam Dynamics With Harmonic Cavities by Using the Code Mbtrack." Proc. 10th International Partile Accelerator Conference (IPAC'19), Melbourne, Australia, 19-24 May 2019. 2019.

[18] Gamelin, Alexis, and Naoto Yamamoto. "Equilibrium Bunch Density Distribution with Multiple Active and Passive RF Cavities." 12th International Particle Accelerator Conference. 2021.

[19] Private communication, to be published.

[20] Venturini, M. (2018). Passive higher-harmonic rf cavities with general settings and multibunch instabilities in electron storage rings. Physical Review Accelerators and Beams, 21(11), 114404.

[21] S.Y, Lee. Accelerator Physics (2nd edition)

5 Appendix A

Here lists some equations about the power comsumption calculation.

$$
\begin{aligned}
V_{gr}^2 &= V_{br}^2 + V_{rf}^2\left(1+tan^2\varphi_Z\right) - 2V_{br}V_{rf}\left(tan\varphi_Z cos\phi_s - sin\phi_s\right) \\
V_{br} &= \frac{R_s I_{im}}{1+\beta} \\
V_{rf} &= \frac{R_s I_0}{1+\beta} \\
P_g &= \frac{(1+\beta)^2}{8\beta R_s} V_{gr}^2 \\
&= \frac{(1+\beta)^2}{8\beta R_s}\left[\left(\frac{R_s I_{im}}{1+\beta}\right)^2 + \left(\frac{R_s I_0}{1+\beta}\right)^2\left(1+tan^2\varphi_Z\right) - \frac{2R_s I_{im}}{1+\beta}\frac{R_s I_0}{1+\beta}\left(tan\varphi_Z cos\phi_s - sin\phi_s\right)\right] \\
&= \frac{R_s}{8\beta}\left[I_{im}^2 + I_0^2(1+tan^2\varphi_Z) - 2I_{im}I_0(tan\varphi_Z cos\phi_s - sin\phi_s)\right] \\
&= \frac{R_s}{8\beta}\left[(I_{im}^2 sin\phi_s^2 + 2I_{im}I_0 sin\phi_s + I_0^2) + (I_{im}^2 cos\phi_s^2 + I_0^2 tan^2\varphi_Z - 2I_{im}I_0 tan\varphi_Z cos\phi_s)\right] \\
&= \frac{R_s}{8\beta}\left[(I_{im}sin\phi_s + I_0)^2 + (I_0 tan\varphi_Z - I_{im}cos\phi_s)^2\right] \\
tan\theta_L &= \frac{I_0 tan\varphi_Z - I_{im}cos\phi_s}{I_{im}sin\phi_s + I_0} \\
P_g &= \frac{R_s}{8\beta}\frac{(I_{im}sin\phi_s + I_0)^2}{cos\theta_L^2}
\end{aligned}
\tag{32}
$$

$$
\begin{aligned}
V_{gr}^2 &= V_{br}^2 + V_{rf}^2\left(1+tan^2\varphi_Z\right) - 2V_{br}V_{rf}\left(tan\varphi_Z cos\phi_s - sin\phi_s\right) \\
&= V_{rf}^2\left[\left(\frac{V_{br}}{V_{rf}}\right)^2 + 1 + tan^2\varphi_Z - 2\frac{V_{br}}{V_{rf}}\left(tan\varphi_Z cos\phi_s - sin\phi_s\right)\right] \\
\frac{V_{br}}{V_{rf}} &= \frac{tan\varphi_Z}{cos\phi_s} \\
V_{gr}^2 &= V_{rf}^2\left[\left(\frac{tan\varphi_Z}{cos\phi_s}\right)^2 + 1 + tan^2\varphi_Z - 2\frac{tan\varphi_Z}{cos\phi_s}\left(tan\varphi_Z cos\phi_s - sin\phi_s\right)\right] \\
&= V_{rf}^2\left[\frac{tan^2\varphi_Z}{cos^2\phi_s} + 1 + tan^2\varphi_Z - 2tan^2\varphi_Z + 2tan\varphi_Z tan\phi_s\right] \\
&= V_{rf}^2\left[\frac{tan^2\varphi_Z}{cos^2\phi_s} + 1 - tan^2\varphi_Z + 2tan\varphi_Z tan\phi_s\right]
\end{aligned}
\tag{33}
$$

$$
\begin{aligned}
V_{gr}^2 &= V_{rf}^2\left[\left(\frac{sin\phi_s}{cos\varphi_Z} + \frac{V_{br}}{V_{rf}}cos\varphi_Z\right)^2 + \left(\frac{cos\phi_s}{cos\varphi_Z} - \frac{V_{br}}{V_{rf}}sin\varphi_Z\right)^2\right] \\
&= V_{rf}^2\left[\left(\frac{sin\phi_s}{cos\varphi_Z} + \frac{tan\varphi_Z}{cos\phi_s}cos\varphi_Z\right)^2 + \left(\frac{cos\phi_s}{cos\varphi_Z} - \frac{tan\varphi_Z}{cos\phi_s}sin\varphi_Z\right)^2\right] \\
&= V_{rf}^2\left[\frac{1}{cos^2\varphi_Z} + \left(\frac{tan\varphi_Z}{cos\phi_s}\right)^2 + 2tan\varphi_Z tan\phi_s - 2tan^2\varphi_Z\right] \\
&= V_{rf}^2\left[\frac{1-2sin^2\varphi_Z}{cos^2\varphi_Z} + \left(\frac{tan\varphi_Z}{cos\phi_s}\right)^2 + 2tan\varphi_Z tan\phi_s\right] \\
&= V_{rf}^2\left[\frac{cos^2\varphi_Z - sin^2\varphi_Z}{cos^2\varphi_Z} + \left(\frac{tan\varphi_Z}{cos\phi_s}\right)^2 + 2tan\varphi_Z tan\phi_s\right] \\
&= V_{rf}^2\left[1 - tan^2\varphi_Z + \left(\frac{tan\varphi_Z}{cos\phi_s}\right)^2 + 2tan\varphi_Z tan\phi_s\right]
\end{aligned}
\tag{34}
$$

6 Appendix B

$$
\begin{aligned}
tan(\varphi_L) &= \frac{I_0 tan(\varphi_z) - I_b cos(\varphi_b)}{I_0 + I_b sin(\varphi_b)} \\
I_g &= \frac{I_0 + I_b sin(\varphi_b)}{cos(\varphi_L)}
\end{aligned}
\tag{35}
$$

$$
\begin{aligned}
V_g &= \frac{I_g}{Y_g + Y_L} \\
P_g &= \frac{1}{2}\frac{Y_L}{(Y_g + Y_L)^2} I_g^2 \\
Y_g &= Y_L = \frac{\beta}{R_s} \\
P_{gmax} &= \frac{1}{2}\frac{R_g}{(1+1)^2} I_g^2 \\
P_{gmax} &= \frac{1}{2} R_g (\frac{I_g}{2})^2 = \frac{1}{8} R_g I_g^2 \\
P_{gmax} &= \frac{R_s}{8\beta} I_g^2 \\
P_{gmax} &= \frac{R_s}{8\beta} \{\frac{I_0 + I_b sin(\varphi_b)}{cos(\varphi_L)}\}^2
\end{aligned}
\tag{36}
$$